Fabrication of aquaporin-based biomimetic membrane for seawater desalination

Ye Li[1†], Saren Qi[1†], Miao Tian[1], Wentalia Widjajanti[1], Rong Wang[1,2*]

1. *Singapore Membrane Technology Centre, Nanyang Environment and Water Research Institute, Nanyang Technological University, 1 Cleantech Loop, Singapore 637141*

2. *School of Civil and Environmental Engineering, Nanyang Technological University, 50 Nanyang Avenue, Singapore 639798*

**Corresponding author: rwang@ntu.edu.sg*

[†] The authors contributed equally

Abstract

This study focuses on enhancing the mechanical strength of aquaporin (AQP)-based biomimetic membranes for seawater desalination. AQP incorporated vesicles were embedded into the selective layer of an optimized thin film composite (TFC) membrane. The resultant membrane, denoted as ASW, exhibited a stable water flux around 20 $L \cdot m^{-2} \cdot h^{-1}$ and 99% NaCl rejection at a constant pressure of 55 bar using 32,000 $mg \cdot L^{-1}$ NaCl solution as feed in reverse osmosis (RO) measurement. The robustness of the ASW membranes were evaluated. The water flux of ASW membrane was almost 100% enhanced compared with that of AQP-free control TFC membranes. The filtration performance of the ASW membrane was further evaluated by a seven-day desalination test using a real seawater secondary effluent collected from a desalination plant in Singapore as feed. To our best knowledge, our study is the first report on the AQP-incorporated RO membrane applied for seawater desalination. A commercial SW30HR membrane was tested in parallel for comparison. The robust ASW membrane exhibited a nearly 80% higher water flux in comparison to the SW30HR membrane with a comparable overall solute rejection, suggesting the advantage and feasibility of Aquaporin based biomimetic membranes for seawater desalination.

Keywords: Biomimetic membrane; Aquaporin; Reverse osmosis; Seawater desalination; Interfacial polymerization.

Highlights:

- The mechanical strength of aquaporin incorporated polyamide layer was characterized with AFM.
- The effects of high pressure compaction and salinity on aquaporin incorporated polyamide layer were investigated.
- The aquaporin based biomimetic membranes were optimized for seawater desalination (SWRO) application.
- A seven-day SWRO measurement of the ASW was conducted using a real seawater secondary effluent.

1. Introduction

Aquaporin (AQP), a water channel protein, has been attracting global interest due to its superior water transport property. Based on molecular dynamics simulation, it possesses a water permeability of 10^8 to 10^9 water molecules per second [1-3]. The incorporation of AQPs into the synthetic membranes is expected to improve membrane performance with increased water permeability while maintaining similar salt rejection [4-8]. So far, several AQP-based biomimetic membranes have been developed in lab-scale for various applications: forward osmosis (FO) [9], nanofiltration (NF) [10-12], and low pressure reverse osmosis (RO) processes [13, 14]. AQP immobilized membranes are also commercially available from Aquaporin A/S for FO and low pressure RO applications [15]. In most studies, aquaporin Z (AqpZ), purified from Escherichia coli cell, was used as it exhibits enhanced water passage with excellent solute retention. In addition, since it can be expressed in a large quantity in Ecoli and has a relatively high stability, the prospect of AqpZ for use in biomimetic membrane fabrication for water treatment application is attractive [8, 16].

In literature, the early studies of biomimetic membranes introduced AQPs to polymeric substrate surfaces by pressure-assisted or magnetic enhanced vesicle adsorption or deposition [17, 18]. Besides, the AQPs-incorporated vesicles can be immobilized into a membrane selective layer by layer-by-layer deposition [18, 19] and cross-linking method [10, 11, 20]. These reported AQPs-reconstituted biomimetic membranes exhibited exceptional water permeability and high salt rejection towards uncharged

small solutes and divalent ions. Immobilization of AQP-vesicles via interfacial polymerization has been demonstrated to be effective for fabricating RO membranes with outstanding rejection against sodium chloride, NaCl [21-23]. The first work of thin film composite (TFC) aquaporin based biomimetic membranes (ABMs) via interfacial polymerization was reported by Zhao et al., [13]. In this study, using a10 mM NaCl solution as feed, the resultant ABM in flat sheet configuration showed nearly 80% water production improvement in comparison with aquaporin-free membranes at the applied pressure of 5 bar. Afterwards, a TFC biomimetic membrane in hollow fiber configuration was developed; approximately 100% increment in water permeability was achieved as compared to the control membrane using a feed solution of 500 $mg \cdot L^{-1}$ NaCl under the hydraulic pressure of 5 bar [9]. Recently, the long-term stability of ABM flat sheet membranes developed by our group was demonstrated using a wastewater secondary effluent as feed under a hydraulic pressure of 5 bar. The stable performance over 100 days of operation suggests the practical feasibility and energy-saving feature of ABMs for wastewater treatment [14].

Despite the fast-moving progress in ABMs development, an important potential application, seawater RO (SWRO) desalination, has not yet been reported. Previous studies normally evaluated the solute separation performances of ABMs using low salinity feed solutions, for example, below 10,000 ppm at relatively low applied pressure of below 15 bar. However, the operating condition for seawater desalination is much harsher (i.e., 32,000 $mg \cdot L^{-1}$ feed salinity at applied pressure over 55 bar), which

imposes more stringent requirements on the quality of ABMs in terms of mechanical strength, water transport property and separation performance, etc.

The aim of our current study is to synthesize aquaporin based seawater (ASW) membrane with enhanced mechanical strength and to evaluate their RO performance under typical seawater desalination condition. The substrate structure of ASW membrane was fine-tuned to ensure its robustness against compaction under high pressure in SWRO process. The selective layer with embedded AQPs of the ASW membrane was systematically characterized by field emission electron microscopy (FEEM), atomic force microscope (AFM), and X-ray photoelectron spectroscopy(XPS). The AFM pin-point mode was firstly utilized to characterize the nanomechanical properties of the selective polyamide layer with and without AQPs. The compaction stability of TFC ASWs and TFC control membranes was evaluated in parallel using a synthetic salt solution at an applied pressure of 55 bar. Finally, the performance of ASW was evaluated using real seawater secondary effluent from a local seawater desalination plant in Singapore as feed for a seven-day period. It is expected that this study could shed a light on developing AQP-based biomimetic membranes capable of being used for seawater desalination.

2. Methodology

2.1 Chemicals and materials used in the study

Unless specified otherwise, all materials and chemicals were used without any further

purification. 1,2-dioleoyl-sn-glycerol-3-phosphocholine (DOPC) lipids (in chloroform, Avanti Polar Lipids, Alabama (USA)) and phosphate buffered saline (PBS) solution (Thermal Fisher Scientific) were used to prepare proteoliposome. Polysulfone resins (PSF, 75 ~ 81 kDa molecular weight, Solvay Advanced Polymers, GA, USA) and N, N-Dimethylformamide (DMF, Merck) were used to prepare dope solutions for membrane substrates. The m-phenylene-diamine (MPD) and Trimesoyl chloride (TMC) were purchased from Sigma Aldrich and adopted as monomers to synthesize the polyamide selective layer. N-hexane (Merck) was employed as the solvent to dissolve TMC. 2-propanol was supplied by Merck as a wetting agent to test the porosity of substrates. Sucrose (Sigma Aldrich) was used as the draw solution for conducting the stopped-flow tests. Sodium chloride (NaCl) was supplied from Merck Millipore (Singapore) to prepare salt solutions for RO tests. A commercial RO membrane with the model name of SW30HR, purchased from Dow FilmTec® (USA), was utilized in the current study for comparison purpose. Ultrapure water was supplied by a Milli-Q water purification system (18.2 MΩ cm).

2.2 Proteoliposome preparation

AQPs were incorporated into the membrane in the form of proteolipsomes (lipid vesicles) [1, 10, 13, 17, 24]. Briefly, 10 mg of DOPC lipid in chloroform was dried a continuous blow of nitrogen gas using an air gun to form an evenly spread thin film on the inner surface of a glass vial. The glass vial with the dried lipid film inside was then stored in a vacuum desiccator for at least 4 hours to ensure the complete removal of

chloroform. Subsequently, 1 mL PBS buffer solution and a certain amount of AQP (the molar ratio of lipid to protein is 400) were added into the glass vial. Afterwards, this mixed solution was vortexed for 40 minutes followed by freeze-thaw with liquid nitrogen for three times. The resultant solution was extruded (Avestin extruder, Avestin, Canada) using a 400-nm polycarbonate filter for 3 times followed by a 200-nm polycarbonate filter for 21 times to obtain proteoliposomes with a uniform size distribution [25].

2.3 Membrane fabrication

2.3.1 Preparation of membrane substrate

Three PSF dope solutions with different polymer concentrations (i.e, 15%, 20% and 24%) were prepared using DMF as organic solvent. The membrane substrates were fabricated via the non-solvent induced phase inversion method. Firstly, one piece of nonwoven fabric was fixed onto a dry and clean glass plate by adhesive tapes. Subsequently, a casting machine (Elcometer Asia Pte Ltd) was employed to evenly spread the polymeric dope solution on the top of a nonwoven fabric that fixed on a glass plate with a gap height of 150 μm. The dope film together with the fabric as well as the glass plate was immediately soaked into a water tank containing clean water at ambient temperature (23±1ºC). After 10-min stabilization time, the PSF membrane substrate was formed and stored in a tank filled with DI water. The soaking water was replaced with fresh pure water several times in a day to minimize the DMF residue in water tank. The resulting three PSF substrates were denoted at

#1, #2 and #3, respectively, following the elevation of polymer concentration in dope solution.

2.3.2 Preparation of the membrane selective layer

The polyamide selective layer of TFC membranes was synthesized via a conventional interfacial polymerization [1, 13]. Briefly, one piece of PSF substrate (150 mm × 200 mm) was fixed onto a hollow stainless steel frame using clamps with the top surface (opposite of the nonwoven fabric) facing up. An aquatic solution containing 1% MPD and 0.33 $mg \cdot mL^{-1}$ proteoliposomes was poured onto the top surface of the PSF substrate and wetted the surface for 20 min, then the excess MPD solution was drained by lifting the membrane coupon vertically, and the membrane surface was subsequently dried using a nitrogen air gun to completely remove large water drops. Then, a 0.15% TMC in n-hexane solution was slowly poured onto the aforesaid substrate to react with the residue of MPD to synthesize a thin polyamide selective layer (the chemical reaction is illustrated in Fig. 1). During this process, proteoliposomes were encapsulated into the polyamide layer. The prepared AQP-incorporated membrane is denoted as ASW. The selective layer without vescicles of the control membrane was synthesized following a same procedure, and was denoted as TFC membrane. The synthesized membranes were subsequently placed in DI water at 4 ºC until further tests.

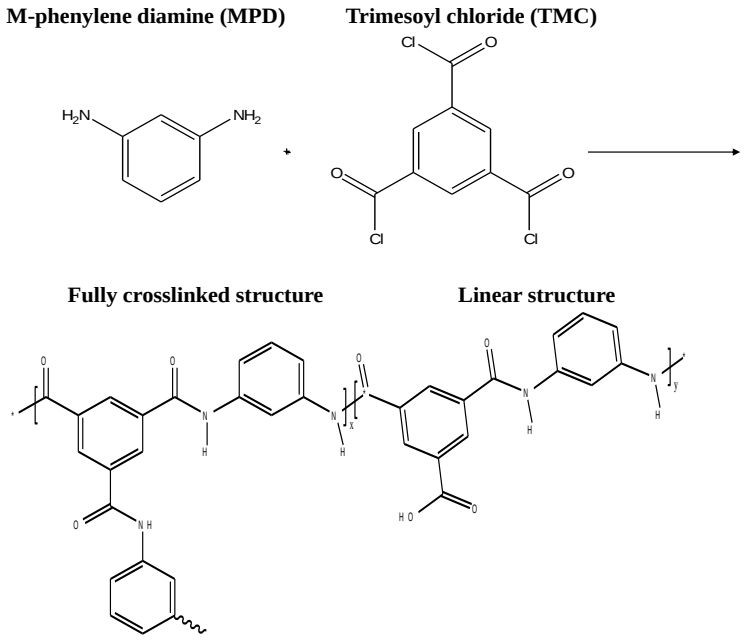

Fig.1. The interfacial polymerization reaction of MPD and TMC (x and y have values between 0 and 1)

2.4 Characterization of liposomes and proteoliposomes

The size distributions of the vesicles were characterized using a Nano Zetasizer (NanoZS, Malvern Instruments Limited, UK) [1, 13]. The permeability of the vesicle was determined using a stopped-flow instrument (SX20 stopped-flow spectrometer, Applied Photophysics, UK) [1, 13]. Briefly, a 0.5 $mg \cdot mL^{-1}$ vesicle solution was prepared and mixed with a 0.6 M sucrose solution with a volume ratio of 1:1 at 25 ^{o}C in the stopped-flow instrument [26, 27]. The volume reduction of proteoliposomes attributed to the outward water transport was detected by a light scattering method. The fitted rate constant k was calculated by using the inbuilt software using a single exponential fitting method to indicate the shrinkage rate of the volume. The water permeability of the vesicle was calculated based on Eq. (1)[16].

$$P_f = \frac{k}{\frac{s}{V_0} \times V_w \times \Delta osm} \quad (1)$$

where k is the average rate constant obtained from the fitting curve, s and V_0 are the surface area and initial volume of one vesicle, respectively, V_w is the partial molar volume of water (0.018 L·mol^{-1}), and Δosm is the difference in osmolarity between the intravesicular and the draw solution.

2.5 Membrane characterization

All membrane samples were dried in a vacuum desiccator at ambient temperature for at least 24 hours before characterization using FESEM (Field-emission scanning electron microscopy, JSM-7600F, JEOL, Japan), AFM (atomic force microscope) and XPS (x-ray photoelectron spectroscopy). The morphologies of the membranes were characterized by FESEM (Field-emission scanning electron microscopy, JSM-7600F, JEOL, Japan). The nonwoven fabrics of the membrane samples were manually peeled off before sample preparation in liquid nitrogen for cross-section characterization. The samples were coated with a platinum thin layer prior to FESEM observation. The surface roughness of the substrates was estimated by AFM (Park XE-100) in a non-contact mode. The AFM was also used to evaluate the elastic modulus and surface roughness of the polyamide selective layer under a pinpoint^{TM} nanomechanical mode. The scanning area was 5 μm × 5 μm with a resolution of 128 pixel. XPS survey scans of the polyamide selective layers were conducted by a Kratos Analytical, AXIS Supra (UK) system using a monochromatic A1 Kα X-ray source (hν=1486.6 eV). The binding

energy was calibrated by adjusting the C1 peak to 284.6 eV. Compositions of elements were analyzed by CasaXPS software.

The porosity of the membrane substrate was estimated by a gravimetric method with 2-propanol as the wetting agent as described in literature [28]. The initial pure water permeability (PWP) of membrane substrates were determined at an applied pressure of 1 bar according to Eq. (2). The low applied pressure was to minimize the severe compaction effect.

$$A = \frac{J_w}{\Delta P} \tag{2}$$

where A is the membrane water permeability; J_w is the water flux calculated based on weighting the permeated water during a certain period; ΔP is the applied pressure.

The PWP of thin film composite membranes were measured using the similar method as the substrates except that the membranes were tested under 55 bar. Solute rejection was determined based on the conductivity difference between the feed and permeate at the same pressure using 2000 mg·L^{-1} sodium chloride as feed solution.

2.6 Evaluation of compaction effect of membrane substrates

The compaction effect of membrane substrate was evaluated using an adapted method from references [29-31]. Briefly, a membrane substrate coupon with an effective area of 42 cm^2 was mounted inside a cross-flow testing cell (CF42 Membrane Cell, Sterlitech). Deionized water was pumped to permeate through the membrane at a

constant cross-flow velocity of ~10 $cm \cdot s^{-1}$ at a constant pressure of 4 bar. Water permeability of each substrate, calculated by the Eq. (2), was recorded at a 30-min time interval for 300 minutes.

2.7 Evaluation of desalination performance of the ASW membrane

The performance of the ASW membrane was evaluated at a hydraulic pressure of 55 bar. The membrane was firstly conditioned for one day using 2000 $mg \cdot L^{-1}$ NaCl as feed. Subsequently, the NaCl concentration of the feed was increased to 32,000 $mg \cdot L^{-1}$ by dosing saturated NaCl solution and the membrane performance with high salinity feed was evaluated for 7 days. The compaction effects of the ASW membranes were studied in comparison to TFC control membrane. Afterwards, the feed water was replaced by seawater secondary effluent (pretreated by a microfiltration process) collected from a Singapore seawater treatment plant. The performance (i.e., water flux and overall rejection) were recorded on a daily basis during a 7-day testing period and a commercial SW30 membrane was tested in parallel for comparison.

3. Results and discussion

3.1 Characterization of the substrates

Three types of polysulfone substrates (i.e, polymer concentrations of dope solutions varied from 15%, 20% to 24%) were prepared via non-solvent induced phase inversion. The casting conditions regarding the drying time in open air, gelation time, and water bath temperature were maintained the same. The dope composition and the physical

properties of the resultant substrates are listed in Table 1. The increase of dope viscosities (in the order of #1, #2, and #3) correlates well with the elevation of the polymer concentrations. Although the casting knife gap was set constant at 150 μm, the thicknesses of the resultant substrates with nonwoven fabrics increase as a result of increased polymer concentrations. As expected, the porosity of the substrate reduces from substrate #1 to #3. Correspondingly, the significant reduction of PWP can be explained by the deceased porosity from Substrate #1 to #3. The three substrates have typical characteristics (i.e., small surface roughness (Ra < 10 nm), relatively high porosity and PWP) required for developing defect-free TFC membranes [32].

Table 1. Basic information of different substrates

Substrate	Dope information			Membrane substrate properties			
	Polymer concentration wt.%	Solvent concentration wt. %	Viscosity [a] (Pa.s)	Thickness [b] (μm)	Porosity (%)	PWP ($L/m^2.h.bar$)	Roughness, R_a (nm)
#1	15	85	0.3 ± 0.1	134 ± 13	87.9 ± 4.1	2831 ± 72	5.8 ± 0.7
#2	20	80	2.2 ± 0.2	140 ± 10	74.0 ± 4.8	77.8 ± 9.0	3.6 ± 0.3
#3	24	76	5.4 ± 0.6	146 ± 9	56.6 ± 4.1	18.9 ± 3.2	2.7 ± 0.3

Notes: [a] the viscosities of the dope solutions were measured at 10 s^{-1} shear rate;

[b] the thicknesses of wetted membrane substrates were measured using a micrometer.

Fig. 2 presents the surface and cross-sectional FESEM images of three substrates. The thick nonwoven support was carefully peeled off from the back side of the substrate sample prior to the characterization for better imaging. The FESEM analysis (Fig. 2a~c) reveals that the #1 has visibly larger surface pores than #2 and #3, which could be

related to the low viscosity of dope solution of #1 (refer to Table 1). The less viscous dope solution reduced the resistance for the non-solvent diffusing into the polymer solution in the phase inversion process. A more rapid and intense diffusion of non-solvent into the dope system resulted in a more porous structure [33, 34]. The cross-section images (Fig. 2d~f) show that all three substrates possess a uniform interconnective sponge-like pore structure. The increase trend of the substrate thickness (without nonwoven support) is consistent with the thickness of substrates measured using a micrometer (listed in Table 1).

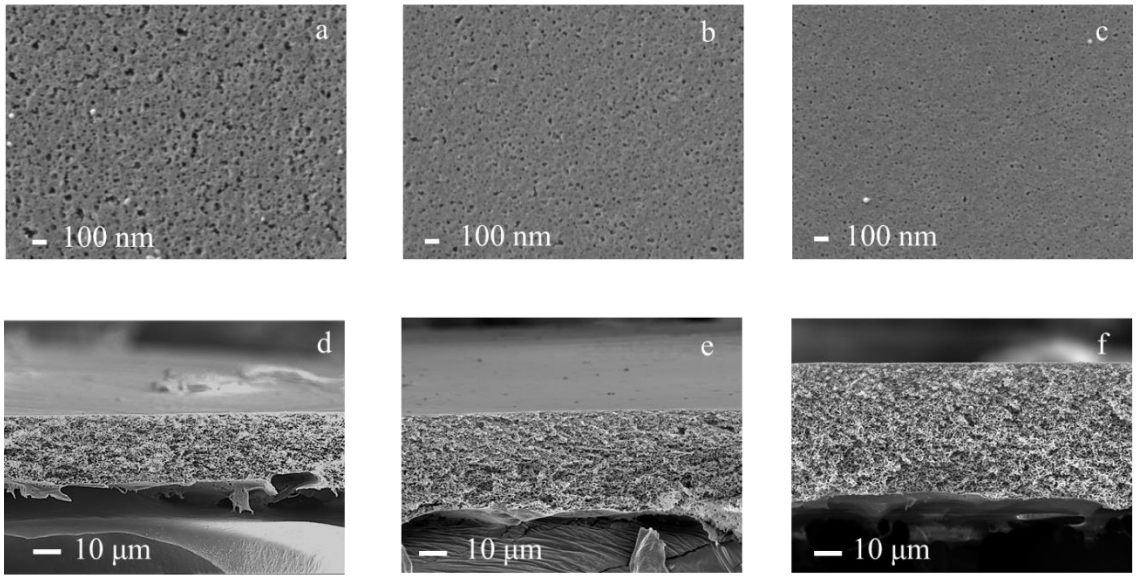

Fig.2. The FESEM images for the substrates prepared from different dope compositions. Top surfaces of (a) #1, (b) #2, (c) #3 and cross-section of (d) #1, (e) #2, (f) #3 are presented.

3.2. Permeability profiles of the substrates under compaction

All the substrates were pressurized under a constant pressure of 4 bar using pure water as feed for a period of 300 minutes. The water flux was measured and recorded at

predetermined time points. Considering the significant difference in the initial water fluxes of three substrates (presented in Table 1), each water flux data was normalized to the initial water flux and the normalized values are shown in Fig. 3. Generally, the water fluxes of all the substrates decline with filtration time as the substrate pore structure become more compacted under pressure. For the substrate #1, compression of the substrate took place as soon as the hydraulic pressure was applied, indicated by the immediate water flux decline. Subsequently, a continuous gradual reduction of water flux was observed for the rest of the compaction period. Such time-dependent compaction phenomenon was also described in references [35, 36]. The water flux decline rate of the substrate #2 was slower than that of #1 (i.e., ~5% reduction for #2 vs. ~35% decline for #1 during 300 minutes). For substrate #3, nearly no reduction of water flux was observed during the entire compaction period (300 minutes). The results suggest that the substrate with a dense structure (low porosity) could produce a more stable water flux under pressure.

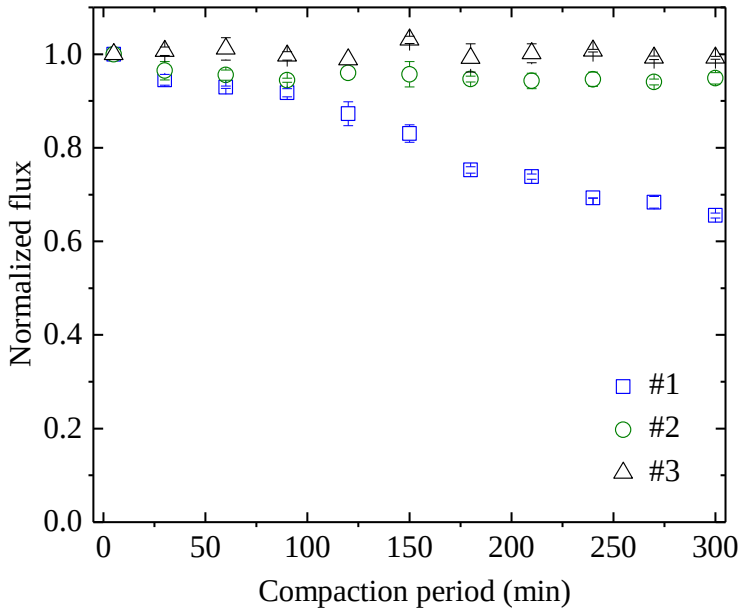

Fig. 3. Flux dependence on compaction for three substrates. Testing conditions: applied pressure was 4 bar and pure water was used as feed.

3.3 Thin film composite membrane performance

Interfacial polymerization method was adopted to form polyamide active layers on top of the substrates. The FESEM images of three thin film composite (TFC) membranes are shown in Fig. 4. Similar surface morphologies were observed for the TFC#1 and TFC#2, which are the typical leaf-like structures for polyamide cross-linked structure [14] . However, an uncommon morphology was revealed for TFC#3, which implies potential difference in the membrane performance.

The results from the filtration measurements are presented in Table 2. The water permeability of three TFC membranes decreased in the order of TFC#1 > TFC#2 > TFC#3; the trend is consistent with the PWPs of the substrates listed in Table 1. On the other hand, TFC#2 exhibited the best salt rejection among the three different TFC membranes. A low salt rejection was observed for TFC#3, which coincides with its unusual surface morphology. It is generally acknowledged that the interfacial polymerization are reactions between two monomers, MPD and TMC, and it mainly occurs in the organic phase. Therefore, the diffusion of the MPD monomer from the substrate voids to the interface to react with TMC plays an important role [37, 38]. As indicated in Fig. 1c, some surface pores were extremely small for substrate #3, which may limit the amount of MPD stored inside the voids, leading to imperfect polyamide

layer formation. Considering both filtration properties and compaction effect, the substrate #2 was selected for the following studies of immobilization of proteoliposomes to fabricate ASW and the TFC#2 was used as a control membrane for comparison purpose.

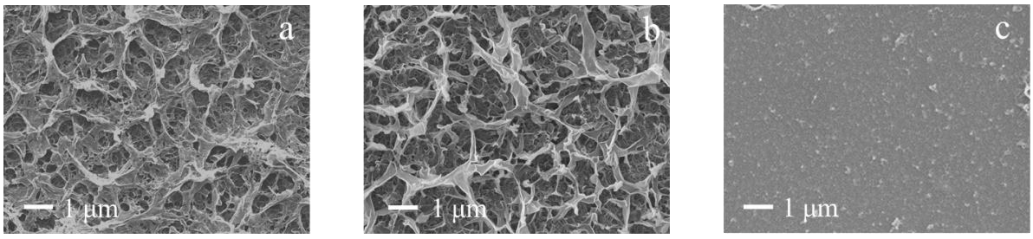

Fig. 4. The FESEM images of the surface of (a) TFC#1, (b) TFC#2, and (c) TFC#3, respectively

Table 2. The intrinsic separation properties of the membranes with different substrates

Membrane type	*A* (LMH/bar)	Rejection (%)*
TFC#1	1.76 ± 0.03	98.78 ± 0.27
TFC#2	1.34 ± 0.11	99.05 ± 0.49
TFC#3	0.94 ± 0.47	71.82 ± 6.56

*Testing conditions: 55 bar pressure and pure water as feed to obtain water permeability (*A*) and 2000 mg·L^{-1} NaCl as feed solution to obtain rejection. Water permeability and rejection were obtained at the initial stage.

3.3 Liposomes and proteoliposomes characterization

DOPC lipid was selected to incorporate the AQPZ to form proteoliposomes due to its excellent stability with solute ions [39]. The size distribution and stopped-flow results of DOPC-based proteoliposomes are presented in Fig. 5. The average size of one

proteolipsome was 137 nm (Fig. 5a) with a small PDI of 0.135. A small PDI indicates the even size distribution of vesicles, reducing error in determining water permeability in stopped-flow tests [14]. Fig. 5b presents the curve with a sharp increment in fluorescence followed by a stable stage. The significant increase of the signal within a short period of < 0.05 s indicates a fast water transportation across the aquaporin [39] while the following stable stage of the signal suggests the good stability of the proteolipsomes under the current solute environment [40].

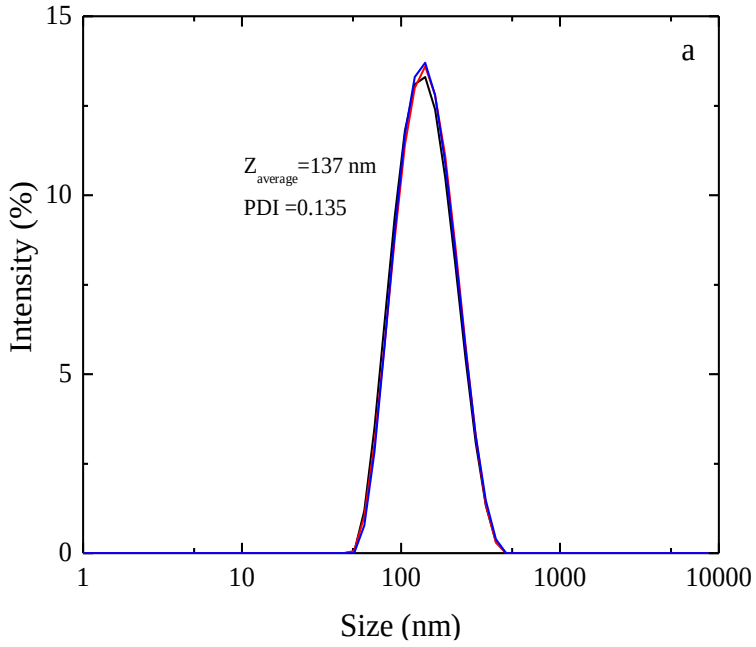

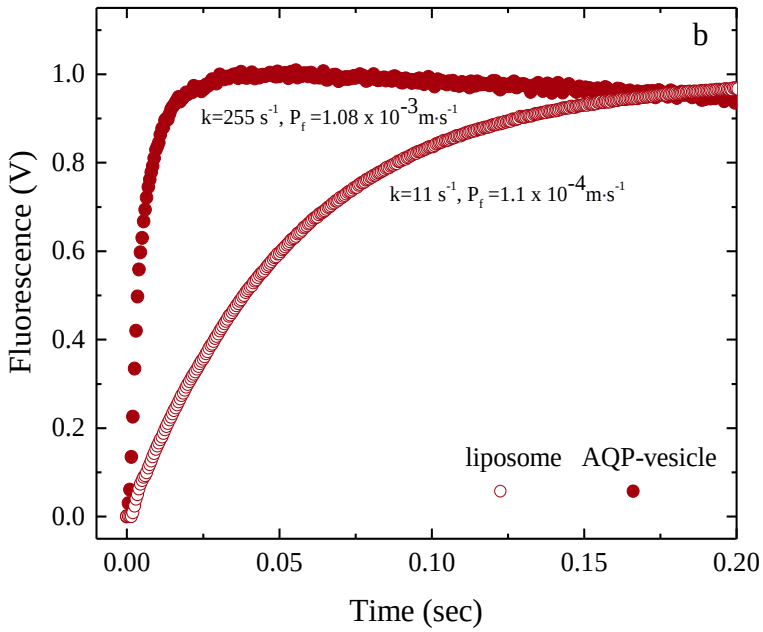

Fig. 5. (a) The size distribution of AQP-vesicle and (b) stopped-flow results using sucrose as draw solution.

3.4. Characterization and separation property of ASW membranes

3.4.1 Characterization of ASW membranes in terms of FESEM, AFM and XPS

The surface morphology of TFC#2 and ASW membrane were imaged by FESEM and shown in Fig. 6a and 6b. Leaf and valley structure can be observed for both types of membranes. The cross sections of the TFC#2 and ASW presenting the top selective layers can be referred to Fig. 6c and 6d. The top layer of the TFC#2 is more smooth compared to that of the ASW. The incorporated proteoliposomes to the polyamide layer caused a significant increment in surface thickness and roughness.

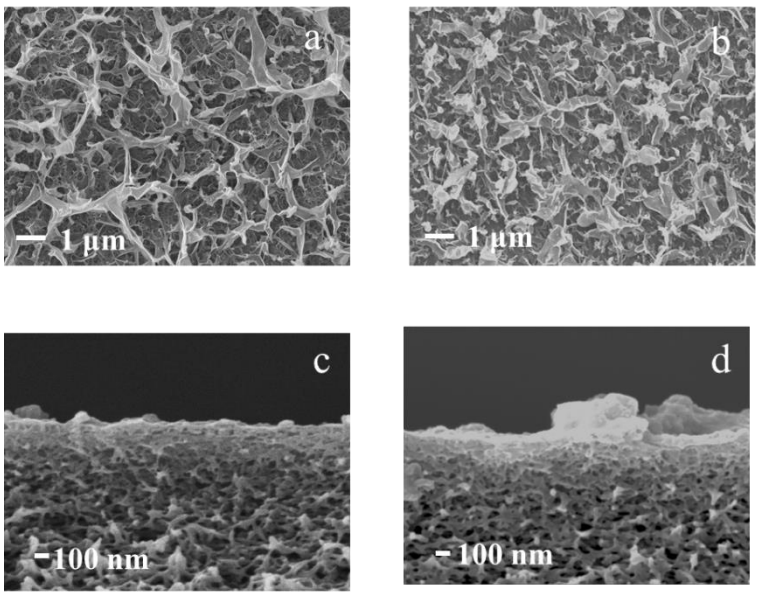

Fig 6. Surface morphology of TFC#2 (a) and ASW membrane (b) and cross section structure of TFC#2 (c) and ASW membrane (d).

The elastic modulus and surface roughness of polyamide selective layers of both ASW and control TFC membranes were determined using AFM under the Pinpoint^{TM} nanomechanical mode, which is a technology extensively applied in material science to determine the mechanical properties of polymer materials [41, 42]. The results listed in Table 3 reveal that mechanical properties of the polyamide layer of ASW membrane with root mean square modulus (E_q) of 0.48 GPa, mean elastic modulus (E_a) of 0.62 GPa, and the maximum elastic modulus (E_z) of 4.87 GPa, which are comparable to those of control TFC membranes considering the mean value and standard deviation. This finding suggests that the incorporation of AQPz-proteoliposomes has minor effect on the mechanical properties of the polyamide layer or even slightly enhance the elastic modulus of the membrane selective layer.

It is interesting to note that the root mean square roughness (R_q), mean roughness (R_a) and maximum peak-to-valley distance (R_z) of ASW are approximately twice the values of the control TFC membrane, indicating a rougher topography of ASW membrane, which may be attributed to the embedment of proteoliposomes (average size of 137 nm in diameter according to Fig. 5a) inside the polyamide layer. This phenomenon could be also observed from Fig. 6d. The areas of the selective layer where proteoliposomes are present have a larger thickness while other areas have an average thickness of an polyamide layer, which results in a significant increase of surface roughness.

Table 3 The elastic modulus and roughness of the polyamide selective layer of TFC and ASW membranes

Membranes	**Elastic modulus (GPa)**			**Surface roughness (nm)**		
	E_q	**E_a**	**E_z**	**R_q**	**R_a**	**R_z**
TFC#2	0.51 ± 0.03	0.41 ± 0.03	3.75 ± 0.26	101 ± 37	78 ± 27	770 ± 269
ASW	0.62 ± 0.17	0.48 ± 0.15	4.87 ± 1.34	238 ± 68	186 ± 53	1426 ± 449

Fig. 7. shows a quantitative mapping of elastic modulus and surface morphology by AFM. The images were acquired by taking high-speed force-distance curves. The darker color represents smaller elastic modulus while the lighter color indicates higher elastic modulus of the membrane surface. The TFC membrane has a more evenly distributed elastic modulus (indicated by the more uniform color pattern in comparison with the ASW membrane. This micro-structure characterization allows for insightful understanding of the morphology and nano-mechanical properties of nanomaterials

such as AQPs in polyamide layers.

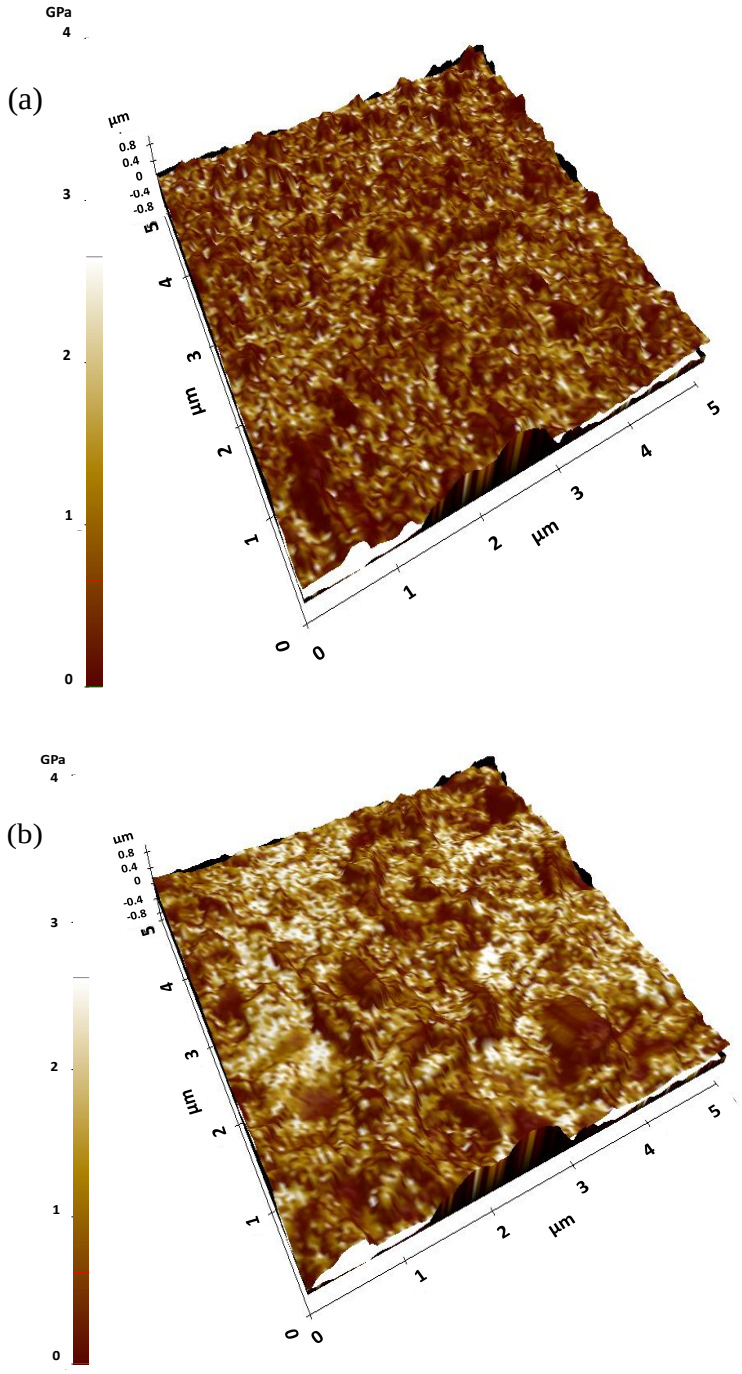

Fig. 7. 3D mapping of (a) TFC#2 (b) ASW membrane under pinpoint mode with the scanning area of 5 µm ×5 µm at 128 pixels

The chemical compositions of polyamide layers of TFC#2 and ASW were analyzed by

XPS survey scan. The only elements that could be detected by XPS spectra were carbon (C), oxygen (O) and nitrogen (N). The compositions of elements could be used to determine the crosslinking degree of the polyamide layer. The crosslinking degree of the polyamide layer was calculated by Eq.(3), which is based on a previous study [43]:

$$\%crosslinking = \frac{x}{x+y} \times 100\% \quad (3)$$

where x and y represent the number of repeat units of fully crosslinked structure and linear structure, respectively. In addition, the ratio of element oxygen to nitrogen (O/N) can also indicate the crosslinking extent of polyamide layers [43, 44]. Referred to Fig. 1, the theoretical value of the O/N ratio is 1 for a fully crosslinking structure (y=0) while the ratio equals to 2 for a fully linear reaction product (x=0). A lower O/N ratio indicates a higher crosslinking extent. The results of compositions of elements are listed in Table 4. The O/N ratios for both TFC#2 and ASW were close to 1 while a slightly higher value was observed for ASW (i.e., 1.1 for TFC#2 and 1.2 for ASW). The crosslinking degree, calculated based on the O/N ratio, shows the same trend. This result suggests that the polyamide selective layers were highly crosslinked for both types of membranes, and the incorporation of AQP vesicles might cause minor defects to the selective layer resulting in a slight decrement in crosslinking degree.

Table 4. Element compositions, oxygen to nitrogen (O/N) ratios and crosslinking degree of the two membranes from XPS analysis

membrane	C (%)	O (%)	N (%)	O/N ratio	crosslinking degree (%)
TFC#2	78.3 ± 0.9	11.1 ± 0.8	10.5 ± 1.5	1.1	86.7

ASW	78.4 ± 0.4	11.3 ± 0.3	10.2 ± 0.1	1.2	84.1
		Theoretical values			
Fully cross-linked	75.0	12.5	12.5	1.0	100.0
Fully linear	71.4	19.1	9.5	2.0	0.0

3.4.2 Pressure compaction and separation properties of ASW membranes

Both ASW and TFC membranes were tested under the same applied pressure of 55 bar with 32,000 $mg \cdot L^{-1}$ as feed for comparison. The water fluxes of two membranes were normalized to the initial water fluxes and the results are presented in Fig. 8. A sharp decrease of water fluxes of both membranes was observed at the initial compaction period (i.e., 1st stage of compaction) due to the instantaneous deformation of substrates at such a high applied pressure [36, 45]. Afterwards, the reduction trend can be fitted into a linear function of the filtration time (i.e., 2nd stage of compaction). In the first stage of compaction, the reduction of water flux of the ASW membrane was more significant than that of the control membrane, suggesting a higher free volume of the selective layer of ASW membrane [45-47]. In the second stage of compaction, the slopes of water flux reduction were similar between ASW membranes and control TFC membranes (i.e., the slope of water flux reduction is -1.0 $L \cdot m^{-2}.h^{-1}.day^{-1}$ and -0.9 $L \cdot m^{-2}.h^{-1}.day^{-1}$ for ASW and TFC membranes, respectively). The slow deformation of the active layer may play a major role in the second compaction stage [48]. This suggests that the immobilization of proteoliposome negligibly affect the mechanical strength of the overall polyamide layer, which is consistent with the AFM characterization in Section 3.4.1.

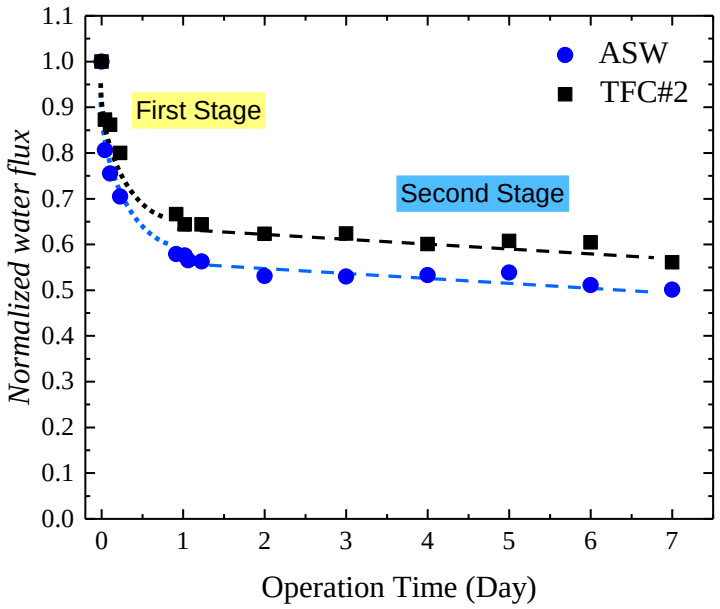

Fig. 8. The compaction performance under the high applied pressure for ASW and control TFC membranes. Testing conditions: applied pressure was 55 bar, and crossflow was 0.1 L·min^{-1}. 2000 mg·L^{-1} NaCl solution was used as feed.

Table 5. lists the water fluxes and salt rejections of ASW and TFC membranes using NaCl solutions with different concentrations (i.e., 2000 mg·L^{-1} and 32,000 mg·L^{-1}). It should be noted that the RO performances of both membranes were evaluated after the 7-day compaction experiments. Under both feed conditions (i.e., 2000 mg·L^{-1} and 32,000 mg·L^{-1}), ASW membrane exhibited nearly 100% water enhancement compared to that of TFC membrane and similar NaCl rejection due to the inherent superior water permeability property of the proteoliposomes (refer to Fig. 5b). Meanwhile, the rejections of both ASW and TFC membranes also slightly decreased using high salinity feed, probably due to the more severe concentration polarization [49, 50].

Table 5. The RO performance of ASW and TFC membranes at the applied pressure of

55 bar*

Membranes	2000 mg·L^{-1}		32,000 mg·L^{-1}	
	Water flux (L/m^2.h)	Rejection (%)	Water flux (L/m^2.h)	Rejection (%)
TFC#2	40.4 ± 1.0	99.7 ± 0.2	11.2 ± 0.5	99.0 ± 0.1
ASW	82.9 ± 2.5	99.3 ± 0.3	21.0 ± 0.4	99.0 ± 0.3

*Water flux and rejection were obtained at the stable stage (i.e., after second stage of compaction)

3.4.3 Performance of ASW membrane using real seawater as feed

The RO performance of the ASW membrane was evaluated using a secondary-treated seawater effluent as feed solution (a typical feed for seawater desalination). The purpose of the test is to further evaluate the feasibility of ASW membrane for seawater desalination application. For comparison purpose, a commercial SW30HR from Dow filmtec was also tested in parallel under the same conditions (i.e., the same applied pressure and the cross-flow rate of 0.125 m·s^{-1}). The water flux and overall solute rejection are shown in Fig. 9. During the testing period, relatively stable water flux and overall rejection (calculated based on the conductivities of the feed and permeate) were observed for three membranes. The ASW membrane exhibited a 22~24 L·m^{-2}h^{-1} of water flux for practical seawater desalination under 55 bar, 80% higher compared to the commercial SW30HR membrane. However, the overall rejection for ASW membrane is lower than that of SW30HR membrane (~98.5% for ASW and ~99.5% for SW30HR).

Table 6. lists the composition of the seawater secondary effluent, the permeate of ASW and the permeate of SW30HR. The concentration of divalent ions ($SO4^{2-}$, Mg^{2+}, Ca^{2+})

for ASW permeate is similar to that for SW30HR permeate water while the ion concentration of monovalent ion is slightly higher for the ASW permeate compared to the SW30 HR. The results indicated that the permeate quality of ASW still needed further improvement to be applicable as seawater desalination RO membrane.

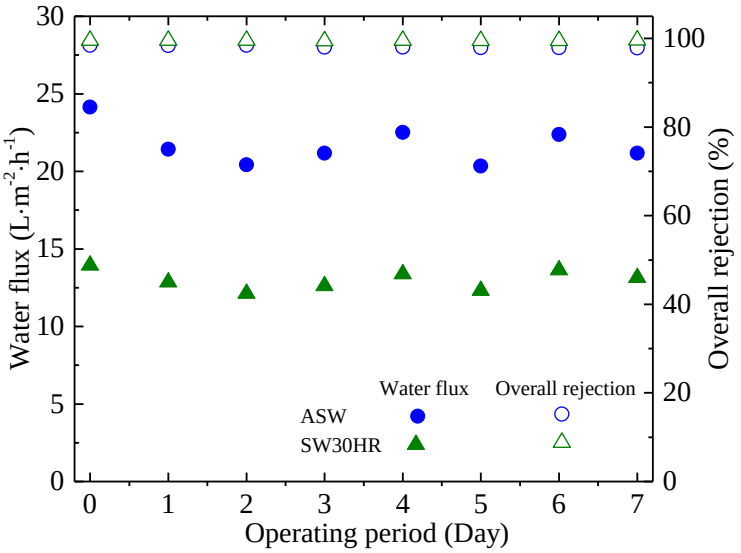

Fig. 9. The desalination performance of ASW membrane using a seawater secondary effluent as feed solution. Testing conditions: Membrane coupons were tested at 55 bar at atmosphere temperature.

Table 6. The ion concentrations of the seawater secondary effluent, the permeate of ASW and of SW30

Water samples	**Ion concentration (ppm)**							
	Cl^-	$SO4^{2-}$	Br^-	Na^+	Mg^{2+}	Ca^{2+}	K^+	B
Feed	16815.5	1873.0	87.8	9640.0	974.5	291.0	500.0	5.2
Permeate (ASW)	222.2	1.3	0.9	129.0	2.1	0.8	6.6	1.2
Permeate (SW30)	63.0	1.3	0.5	37.0	0.9	0.5	2.7	0.4

The ABMs that were fabricated for NF, low pressure RO (LPRO), SWRO applications and subsequently reported in literature are summarized in Table 7. In most cases, the

encapsulation of AQP-vesicles to the polyamide skin of the membrane enhanced the water permeability compared to the vesicle-free control membranes or the AQP-free lipid-based membranes. It can be seen that our study is the first attempt to apply AQPs for membrane fabrication intended for use in seawater desalination. The resultant ASW membrane achieved 91% increment in water permeability as compared with the control membrane without AQP incorporation, when using real sweater secondary effluent as feed for testing. The result is encouraging.

Notably, it is challenging but imperative to further improve the selectivity of ASW membrane, as the removal of heavy metals and other toxic contaminants should also be taken into consideration for the ASW membrane design [51, 52]. In addition, a long-term test with comprehensive fouling study could provide more information on the feasibility of ASW membrane for this application, as ASW membrane with a high surface roughness might be prone to fouling [53].

Table 7. Summary of lab-synthesized ABM for pressure-driven applications

Application	**Increment in A^a (%)**	**Substrate**	**Fabrication approach**	**Vesicle**	**Operating pressure (bar)**	**Reference**
SWRO	91	polysulfone	interfacial polymerization	AQP-DOPC	55	current study
LPRO	54	polysulfone	interfacial polymerization	AQP-Ecoli	10	[14]
LPRO	166	polyetherimide	interfacial polymerization	AQP-Ecoli	5	[9]
LPRO	25	polysulfone	interfacial polymerization	AQP-DOPC	5	[13]
NF	53[b]	Polyacrylonitrile	layer-by-layer	AQP-DOPC	4	[54]

NF	60	Polyacrylonitrile	layer-by-layer	AqpZ-POPC/POPG	4	[55]
NF	65	Polyacrylonitrile	chemical crosslinking	AQP-DOPC	5	[11]

Notes: [a] the increase of *A* was based on the comparison between AQP-vesicle embedded membranes and the vesicle-free control membranes;
[b] the increase of *A* of AQP-vesicle embedded membrane was in comparison with lipid embedded control membranes.

4. Conclusions

A robust aquaporin-based biomimetic membrane was successfully fabricated on an optimized polysulfone substrate. The mechanical stability and seawater desalination performance of the ASW membrane were evaluated in the current study. Several findings are summarized as follows:

(1) The morphology, water permeability, porosity and compaction effect of the substrate prepared from dope solutions with different polymer concentrations were systemically investigated.

(2) The incorporation of aquaporin-based proteoliposomes into the selective layer facilitates nearly 100% increment of water flux of the TFC membrane attributed to the superior water permeable channels in proteoliposomes. Besides, the presence of proteoliposomes has negligible impact on the compaction of the membrane as compared with the AqpZ free membranes.

(3) The polyamide layer with AqpZ immobilized was demonstrated to be stable in the desalination tests using a real second effluent of seawater as feed. The high water flux and acceptable rejection were maintained stable for 7 days of testing time, suggesting the great potential of the ASW membranes for real seawater desalination.

Acknowledgments

The research is conducted under the IAF-PP project supported by the Singapore National Research Foundation and PUB, Singapore's National Water Agency. Funding support from the Singapore Economic Development Board to the Singapore Membrane Technology Centre is also gratefully acknowledged.

References

[1] C.Y. Tang, Y. Zhao, R. Wang, C. Hélix-Nielsen, A.G. Fane, Desalination by biomimetic aquaporin membranes: Review of status and prospects, Desalination, 308 (2013) 34-40.

[2] M.L. Zeidel, S. Nielsen, B.L. Smith, S.V. Ambudkar, A.B. Maunsbach, P. Agre, Ultrastructure, Pharmacologic Inhibition, and Transport Selectivity of Aquaporin CHIP in Proteoliposomes, Biochemistry, 33 (1994) 1606-1615.

[3] P. Agre, Aquaporin Water Channels (Nobel Lecture), Angewandte Chemie International Edition, 43 (2004) 4278-4290.

[4] M. Kumar, M. Grzelakowski, J. Zilles, M. Clark, W. Meier, Highly permeable polymeric membranes based on the incorporation of the functional water channel protein Aquaporin Z, Proceedings of the National Academy of Sciences of the United States of America, 104 (2007) 20719-20724.

[5] A. Giwa, S.W. Hasan, A. Yousuf, S. Chakraborty, D.J. Johnson, N. Hilal, Biomimetic membranes: A critical review of recent progress, Desalination, 420 (2017) 403-424.

[6] G. Calamita, W.R. Bishai, G.M. Preston, W.B. Guggino, P. Agre, Molecular cloning and characterization of AqpZ, a water channel from Escherichia coli, Journal of Biological Chemistry, 270 (1995) 29063-29066.

[7] D.F. Savage, P.F. Egea, Y. Robles-Colmenares, J.D. O'Connell Iii, R.M. Stroud, Architecture and selectivity in aquaporins: 2.5 Å X-ray structure of aquaporin Z, PLoS Biology, 1 (2003).

[8] M. Kumar, M. Grzelakowski, J. Zilles, M. Clark, W. Meier, Highly permeable polymeric membranes based on the incorporation of the functional water channel protein Aquaporin Z, Proceedings of the National Academy of Sciences, 104 (2007) 20719-20724.

[9] X. Li, S. Chou, R. Wang, L. Shi, W. Fang, G. Chaitra, C.Y. Tang, J. Torres, X. Hu, A.G. Fane, Nature gives the best solution for desalination: Aquaporin-based hollow fiber composite membrane with superior performance, Journal of Membrane Science, 494 (2015) 68-77.

[10] X. Li, R. Wang, F. Wicaksana, C. Tang, J. Torres, A.G. Fane, Preparation of high performance nanofiltration (NF) membranes incorporated with aquaporin Z, Journal of Membrane Science, 450 (2014) 181-188.

[11] G. Sun, T.-S. Chung, K. Jeyaseelan, A. Armugam, Stabilization and immobilization of aquaporin reconstituted lipid vesicles for water purification, Colloids and Surfaces B: Biointerfaces, 102 (2013) 466-471.

[12] P.S. Zhong, T.-S. Chung, K. Jeyaseelan, A. Armugam, Aquaporin-embedded biomimetic membranes for nanofiltration, Journal of Membrane Science, 407-408 (2012) 27-33.

[13] Y. Zhao, C. Qiu, X. Li, A. Vararattanavech, W. Shen, J. Torres, C. Hélix-Nielsen, R. Wang, X. Hu, A.G. Fane, C.Y. Tang, Synthesis of robust and high-performance aquaporin-based biomimetic membranes by interfacial polymerization-membrane preparation and RO performance characterization, Journal of Membrane Science, 423-424 (2012) 422-428.

[14] S. Qi, R. Wang, G.K.M. Chaitra, J. Torres, X. Hu, A.G. Fane, Aquaporin-based biomimetic reverse osmosis membranes: Stability and long term performance, Journal of Membrane Science, 508 (2016) 94-103.

[15] Z. Li, R. Valladares Linares, S. Bucs, L. Fortunato, C. Hélix-Nielsen, J.S. Vrouwenvelder, N. Ghaffour, T. Leiknes, G. Amy, Aquaporin based biomimetic membrane in forward osmosis: Chemical cleaning resistance and practical operation, Desalination, 420 (2017) 208-215.

[16] M.J. Borgnia, D. Kozono, G. Calamita, P.C. Maloney, P. Agre, Functional reconstitution and characterization of AqpZ, the E. coli water channel protein11Edited by W. Baumeister, Journal of Molecular Biology, 291 (1999) 1169-1179.

[17] X. Li, R. Wang, C. Tang, A. Vararattanavech, Y. Zhao, J. Torres, T. Fane, Preparation of supported lipid membranes for aquaporin Z incorporation, Colloids and Surfaces B: Biointerfaces, 94 (2012) 333-340.

[18] G. Sun, T.-S. Chung, N. Chen, X. Lu, Q. Zhao, Highly permeable aquaporin-embedded biomimetic membranes featuring a magnetic-aided approach, RSC Advances, 3 (2013) 9178-9184.

[19] G. Sun, T.-S. Chung, K. Jeyaseelan, A. Armugam, A layer-by-layer self-assembly approach to developing an aquaporin-embedded mixed matrix membrane, RSC Advances, 3 (2013) 473.

[20] W. Xie, F. He, B. Wang, T.-S. Chung, K. Jeyaseelan, A. Armugam, Y.W. Tong, An aquaporin-based vesicle-embedded polymeric membrane for low energy water filtration, Journal of Materials Chemistry A, 1 (2013) 7592-7600.

[21] J. Zhao, X. Zhao, Z. Jiang, Z. Li, X. Fan, J. Zhu, H. Wu, Y. Su, D. Yang, F. Pan, J. Shi, Biomimetic and bioinspired membranes: Preparation and application, Progress in Polymer Science, 39 (2014) 1668-1720.

[22] J. Habel, M. Hansen, S. Kynde, N. Larsen, S.R. Midtgaard, G.V. Jensen, J. Bomholt, A. Ogbonna, K. Almdal, A. Schulz, C. Hélix-Nielsen, Aquaporin-based biomimetic polymeric membranes: Approaches and challenges, Membranes, 5 (2015) 307-351.

[23] C. Tang, Z. Wang, I. Petrinić, A.G. Fane, C. Hélix-Nielsen, Biomimetic aquaporin membranes coming of age, Desalination, 368 (2015) 89-105.

[24] X. Li, R. Wang, F. Wicaksana, Y. Zhao, C. Tang, J. Torres, A.G. Fane, Fusion behaviour of aquaporin Z incorporated proteoliposomes investigated by quartz crystal microbalance with dissipation (QCM-D), Colloids and Surfaces B: Biointerfaces, 111 (2013) 446-452.

[25] J.S. Hansen, V. Ardcharaporn, P. Inés, J.G. Per, B. Julie, T. Jaume, E. Jenny, C.H. Nielsen, Interaction between sodium dodecyl sulfate and membrane reconstituted aquaporins: A comparative study of spinach SoPIP2;1 and E. coli AqpZ, Biochimica et Biophysica Acta, 1808 (2011) 8.

[26] J.B. Mario, K. David, P. Agre, Functional Reconstitution and Characterization of AqpZ, the E. coli Water Channel Protein, J. Mol. Biol, (1999).

[27] M. Kumar, M. Grzelakowski, J. Zilles, M. Clark, W. Meier, Highly permeable polymeric membranes based on the incorporation of the functional water channel protein Aquaporin Z, PNAS, 104 (2007) 6.

[28] J. Wei, C. Qiu, C.Y. Tang, R. Wang, A.G. Fane, Synthesis and characterization of flat-sheet thin film composite forward osmosis membranes, Journal of Membrane Science, 372 (2011) 292-302.

[29] H.R. Lohokare, Y.S. Bhole, U.K. Kharul, Effect of support material on ultrafiltration membrane performance, Journal of Applied Polymer Science, 99 (2006) 3389-3395.

[30] K.M. Persson, V. Gekas, G. Trägårdh, Study of membrane compaction and its influence on ultrafiltration water permeability, Journal of Membrane Science, 100 (1995) 155-162.

[31] G. Arthanareeswaran, P. Thanikaivelan, K. Srinivasn, D. Mohan, M. Rajendran, Synthesis, characterization and thermal studies on cellulose acetate membranes with additive, European Polymer Journal, 40 (2004) 2153-2159.

[32] M.F. Jimenez-Solomon, P. Gorgojo, M. Munoz-Ibanez, A.G. Livingston, Beneath the surface: Influence of supports on thin film composite membranes by interfacial polymerization for organic solvent nanofiltration, Journal of Membrane Science, 448 (2013) 102-113.

[33] H. Sofiah, A. Nora'aini, M.A. Marinah, The influence of polymer concentration on performance and morphology of asymmetric ultrafiltration membrane for lysozyme separation, Journal of Applied Sciences, 10 (2010) 3325-3330.

[34] A.L. Ahmad, M. Sarif, S. Ismail, Development of an integrally skinned ultrafiltration membrane for wastewater treatment: Effect of different formulations of PSf/NMP/PVP on flux and rejection, Desalination, 179 (2005) 257-263.

[35] D.M. Bohonak, A.L. Zydney, Compaction and permeability effects with virus filtration membranes, Journal of Membrane Science, 254 (2005) 71-79.

[36] V.R. Tarnawski, P. Jelen, Estimation of compaction and fouling effects during membrane processing of cottage cheese whey, Journal of Food Engineering, 5 (1986) 75-90.

[37] J. Jegal, S.G. Min, K.-H. Lee, Factors affecting the interfacial polymerization of polyamide active layers for the formation of polyamide composite membranes, Journal of Applied Polymer Science, 86 (2002) 2781-2787.

[38] V. Freger, Kinetics of Film Formation by Interfacial Polycondensation, Langmuir, 21 (2005) 1884-1894.

[39] Y. Zhao, A. Vararattanavech, X. Li, C. HélixNielsen, T. Vissing, J. Torres, R. Wang, A.G. Fane, C.Y. Tang, Effects of Proteoliposome Composition and Draw Solution Types on Separation Performance of Aquaporin-Based Proteoliposomes: Implications for Seawater Desalination Using Aquaporin-Based Biomimetic Membranes, Environmental Science & Technology, 47 (2013) 1496-1503.

[40] Y.X. Shen, W. Si, M. Erbakan, K. Decker, R. De Zorzi, P.O. Saboe, Y.J. Kang, S. Majd, P.J. Butler, T. Walz, A. Aksimentiev, J.L. Hou, M. Kumar, D.A. Weitz, Highly permeable artificial water channels that can self-assemble into two-dimensional arrays, Proceedings of the National Academy of Sciences of the United States of America, 112 (2015) 9810-9815.

[41] W.C. Oliver, G.M. Pharr, Measurement of hardness and elastic modulus by instrumented indentation: Advances in understanding and refinements to methodology,

Journal of Materials Research, 19 (2011) 3-20.

[42] W.C. Oliver, G.M. Pharr, An improved technique for determining hardness and elastic modulus using load and displacement sensing indentation experiments, Journal of Materials Research, 7 (2011) 1564-1583.

[43] O. Akin, F. Temelli, Probing the hydrophobicity of commercial reverse osmosis membranes produced by interfacial polymerization using contact angle, XPS, FTIR, FE-SEM and AFM, Desalination, 278 (2011) 387-396.

[44] C.Y. Tang, Y.-N. Kwon, J.O. Leckie, Probing the nano- and micro-scales of reverse osmosis membranes—A comprehensive characterization of physiochemical properties of uncoated and coated membranes by XPS, TEM, ATR-FTIR, and streaming potential measurements, Journal of Membrane Science, 287 (2007) 146-156.

[45] R.A. Peterson, A.R. Greenberg, L.J. Bond, W.B. Krantz, Use of ultrasonic TDR for real-time noninvasive measurement of compressive strain during membrane compaction, Desalination, 116 (1998) 115-122.

[46] Y.A. Hussain, M.H. Al-Saleh, S.S. Ar-Ratrout, The effect of active layer non-uniformity on the flux and compaction of TFC membranes, Desalination, 328 (2013) 17-23.

[47] V.E. Reinsch, A.R. Greenberg, S.S. Kelley, R. Peterson, L.J. Bond, A new technique for the simultaneous, real-time measurement of membrane compaction and performance during exposure to high-pressure gas, Journal of Membrane Science, 171 (2000) 217-228.

[48] H. Ohya, An expression method of compaction effects on reverse osmosis

membranes at high pressure operation, Desalination, 26 (1978) 163-174.

[49] V. Gekas, B. Hallström, Mass transfer in the membrane concentration polarization layer under turbulent cross flow. I. Critical literature review and adaptation of existing sherwood correlations to membrane operations, Journal of Membrane Science, 30 (1987) 153-170.

[50] S. Sablani, M. Goosen, R. Al-Belushi, M. Wilf, Concentration polarization in ultrafiltration and reverse osmosis: A critical review, Desalination, 141 (2001) 269-289.

[51] J.R. Werber, A. Deshmukh, M. Elimelech, The Critical Need for Increased Selectivity, Not Increased Water Permeability, for Desalination Membranes, Environmental Science & Technology Letters, 3 (2016) 112-120.

[52] J.R. Werber, C.J. Porter, M. Elimelech, A Path to Ultraselectivity: Support Layer Properties To Maximize Performance of Biomimetic Desalination Membranes, Environ Sci Technol, 52 (2018) 10737-10747.

[53] M. Elimelech, Z. Xiaohua, A.E. Childress, H. Seungkwan, Role of membrane surface morphology in colloidal fouling of cellulose acetate and composite aromatic polyamide reverse osmosis membranes, Journal of Membrane Science, 127 (1997) 101-109.

[54] M. Wang, Z. Wang, X. Wang, S. Wang, W. Ding, C. Gao, Layer-by-Layer Assembly of Aquaporin Z-Incorporated Biomimetic Membranes for Water Purification, Environmental Science & Technology, 49 (2015) 3761-3768.

[55] G. Sun, T.-S. Chung, K. Jeyaseelan, A. Armugam, A layer-by-layer self-assembly approach to developing an aquaporin-embedded mixed matrix membrane, RSC

Advances, 3 (2013) 473-481.